AMERICAN
METEOROLOGICAL
SOCIETY

Journal of Climate

EARLY ONLINE RELEASE

This is a preliminary PDF of the author-produced manuscript that has been peer-reviewed and accepted for publication. Since it is being posted so soon after acceptance, it has not yet been copyedited, formatted, or processed by AMS Publications. This preliminary version of the manuscript may be downloaded, distributed, and cited, but please be aware that there will be visual differences and possibly some content differences between this version and the final published version.

The DOI for this manuscript is doi: 10.1175/JCLI-D-13-00468.1

The final published version of this manuscript will replace the preliminary version at the above DOI once it is available.

If you would like to cite this EOR in a separate work, please use the following full citation:

Yang, Q., L. Leung, S. Rauscher, T. Ringler, and M. Taylor, 2013: Atmospheric moisture budget and spatial resolution dependence of precipitation extremes in aqua-planet simulations. J. Climate. doi:10.1175/JCLI-D-13-00468.1, in press.

© 2013 American Meteorological Society

Manuscript (non-LaTeX)
Click here to download Manuscript (non-LaTeX): extreme.paper.wfigures.revision.v6.nov2013.docx

Atmospheric moisture budget and spatial resolution dependence of precipitation extremes in aqua-planet simulations

Qing Yang[1*], L. Ruby Leung[1], Sara A. Rauscher[2], Todd D. Ringler[2], and Mark A. Taylor[3]

[1]Pacific Northwest National Laboratory, Richland, Washington, USA

[2]Los Alamos National Laboratory, Los Alamos, New Mexico, USA

[3]Sandia National Laboratories, Albuquerque, NM, USA

*Corresponding author: 902 Battelle Boulevard, P.O. Box 999, MSIN K9-30, Richland, WA 99352, USA; qing.yang@pnnl.gov

PRELIMINARY ACCEPTED VERSION

ABSTRACT

This study investigates the moisture budgets and resolution dependency of precipitation extremes in an aqua-planet framework based on the Community Atmosphere Model (CAM4). Moisture budgets from simulations using two different dynamical cores, the Model for Prediction Across Scales - Atmosphere (MPAS-A) and High Order Method Modeling Environment (HOMME), but the same physics parameterizations suggest that during precipitation extremes the intensity of precipitation is approximately balanced by the vertical advective moisture transport. The resolution dependency in extremes from simulations at their native grid resolution originates from that of vertical moisture transport, which is mainly explained by changes in dynamics (related to omega) with resolution. When assessed at the same grid scale by area-weighted averaging the fine-resolution simulations to the coarse grids, simulations with either dynamical core still demonstrate resolution dependency in extreme precipitation with no convergence over the tropics, but convergence occurs at a wide range of latitudes over the extra-tropics. The use of lower temporal frequency data (i.e., daily versus 6-hourly) reduces the resolution dependency. Although thermodynamic (moisture) changes become significant in offsetting the effect of dynamics when assessed at the same grid scale, especially over the extra-tropics, changes in dynamics with resolution are still large and explain most of the resolution dependency during extremes. This suggests that the effects of sub-grid scale variability of omega and vertical moisture transport during extremes are not adequately parameterized by the model at coarse resolution. The aqua-planet framework and analysis described in this study provide an important metric for

assessing sensitivities of cloud parameterizations to spatial resolution and dynamical cores under extreme conditions.

1. Introduction

Increasing numbers of record-breaking and devastating hydrological extremes in the past decade (Coumou and Rahmstorf, 2012) has raised concerns that such extremes may have intensified in a warmer world (Allan and Soden, 2008). Climate models have been used to attribute the causes of precipitation extremes (PEs) and to project the frequency and intensity of these events in the future. However, a known bias in global climate models is the prevalence of drizzle and under-prediction of heavy precipitation due partly to the coarse spatial resolution of the models (Stephens et al. 2010). Also climate models are known to exhibit varying degrees of dependency on parameterization and model resolution (e.g., Boyle and Klein, 2010; Williamson, 1999). Hence, significant uncertainties exist in future PEs projected by an ensemble of climate models (Randall et al., 2007), although they generally project intensification of the hydrological cycle, with larger extremes in both floods and droughts (Held and Soden, 2006).

Precipitation is difficult to characterize due to its high variability across nearly all temporal and spatial scales (Berg et al., 2013). Precipitation extremes are associated with low-frequency variability in the flow field that occasionally results in large anomalous horizontal moisture flux convergence or divergence (Held and Soden, 2006). Although PEs can be defined rather unambiguously using statistical measures, the physical and dynamical mechanisms associated with PEs vary and are still not fully understood. Furthermore, global climate model (GCM) parameterizations are typically developed and tested more extensively to reproduce large-scale climatological mean conditions. Williamson (2013) found that using typical parameter values of convective time scales (e.g., 1–2 hours) assumed in shallow and convective parameterizations can cause

unrealistic development of grid-point storms producing heavy precipitation in high-resolution GCM simulations. In addition, mass-flux parameterizations (e.g., Zhang and McFarlane, 1995) assume that the fractional area covered by convective clouds in a grid cell is far less than 1. The validity of this assumption becomes questionable as GCMs are applied at finer resolutions, making it necessary for parameterizations to adapt to a wider range of model resolutions (Arakawa et al., 2011), with implications to simulating the full spectrum of precipitation intensity.

With increasing high performance computational resources, high-resolution modeling provides a promising path to improving simulations of PE. However, more research is needed to understand the sensitivity of PE to model resolutions and physics parameterizations. Williamson (1999) showed that physics parameterizations, not dynamics, are responsible for the sensitivity of model results to horizontal resolution in his GCM simulations. Li et al. (2011a, b) used an aqua-planet version of Community Atmospheric Model (CAM3) and found that PEs are more sensitive to horizontal resolution than the mean precipitation, suggesting that the effects of horizontal resolution must be taken into account in developing robust projections of PEs. Without improvement in physics representation, increasing resolution alone may only provide limited improvement in climate models skills (Buizza, 2010). Understanding the resolution dependency of PEs is an important first step towards achieving scalable and robust simulations.

This study aims to characterize the resolution dependency of extreme precipitation intensity and the variation of this dependency with dynamical cores, and to estimate the relative contributions of thermodynamics and dynamics to that resolution

dependency. The study is conducted using an aqua-planet framework that simplifies the analyses and interpretations in the absence of complex land-ocean contrast and land surface heterogeneity. Detailed moisture budget analyses have been performed to compare simulations produced by the Community Atmosphere Model version 4 (CAM4) (Neale et al. 2010) with two different dynamical cores applied at a range of spatial resolution, all using the same physics parameterizations.

The rest of this paper is organized as follows. Section 2 describes the model, the aqua-planet experiments, and the simulation outputs. Section 3 discusses the analytical methods including the definition of extremes, the moisture budget equation, and the breakdowns of moisture transport to mean flow and eddy components. The characteristics of the resolution dependency in PEs and attribution of the resolution dependency are presented in Section 4. The last section (Section 5) summarizes the main conclusions from this study.

2. Model description and experiments

As part of the collaborative Robust Regional Modeling project (Leung et al., 2013) supported by the U.S. Department of Energy (DOE), a set of aqua-planet simulations have been conducted using the CAM4 physics package and three different dynamical cores: Model for Prediction Across Scales Atmosphere (MPAS-A) (Rauscher et al. 2013), High-Order Method Modeling Environment (HOMME) (Taylor and Fournier 2010; Evans et al., 2013), and Spectral Eulerian (EUL). Detailed model description and configuration can be found in Rauscher et al. (2013), O'Brien et al. (2013), and Leung et al. (2013). This study primarily uses simulations from the newer

dynamical core MPAS-A, with some comparison with HOMME to provide insights on the impacts of dynamical cores on PE.

Briefly, in CAM4 the convective parameterization includes both a deep and a shallow moisture convection schemes. The shallow moist convective scheme by Hack et al. (1994) as described in Neale et al. (2010) is used to simulate shallow and middle-level convections. The modified deep convection scheme of Zhang and McFarlane (1995) based on a plume ensemble approach in which convective scale updrafts occur when the convective available potential energy (CAPE) exceeds a threshold value in the lower troposphere (Neale et al., 2010) is used to simulate deep convective cloud and precipitation.

Non-convective cloud processes are parameterized by the Rasch-Kristjansson scheme (Rasch and Kristjansson, 1998) with improved treatment of condensation and evaporation as described in Zhang et al. (2003). The Rasch-Kristjansson scheme is a bulk microphysical scheme with both macro- and micro- components. It represents prognostic condensate with exchange between condensate and vapor and the associated temperature change, and includes a bulk representation of conversion from condensate to precipitation (Neale et al., 2010).

The simulations used the default configuration in CAM4 consisting of 26 vertical levels in a sigma vertical coordinate with varying horizontal resolutions. Identical physics parameterizations with no adjustment for dynamical cores or spatial resolutions were used in all simulations. A set of four experiments was conducted for each dynamical core with varying resolutions (equivalent 240, 120, 60, and 30 km for MPAS-A; 220, 110, 55,

28 km for HOMME; and T42, T85, T170, and T340 for EUL). The CAM physical time step was set to be 10-min for all experiments.

In the aqua-planet experiments, the prescribed sea-surface temperature (SST) is symmetric about the equator and decreases from a peak value of 27°C at the equator to 0°C above 60° latitude (Φ) according to the following equation in Neale and Hoskins (2000):

$$T_s(\phi) = 27\left(1 - sin^2\left(\frac{3\Phi}{2}\right)\right): \ -\frac{\pi}{3} < \Phi < \frac{\pi}{3}$$

$$\text{or } 0°\text{C} \ : \text{otherwise}$$

Solar radiation is fixed to equinox solar conditions and is symmetric in the two hemispheres. Thus, seasonal and interannual variations are not represented in these aqua-planet experiments.

The analysis in this study mainly uses the archived 6-hourly data, although daily data were used to test the consistency between the scale dependency of extremes determined based on 6-hourly data and that arrived using lower temporal frequency data. The simulations with the MPAS-A dynamical core uses hexagonal grids, and they have been remapped to the corresponding Finite-Volume (FV) grid with equivalent resolution using conservative remapping described in Rauscher et al. (2013) to facilitate the analysis. Similar mapping to FV grid has also been conducted for simulations with the HOMME dynamical core. Each experiment was 5-year long and the first six-month was considered the spin-up period and excluded from the analysis. The moisture budget analysis (Section 4.2) is based on the 6-hourly data from the third-year simulation, while the rest of the scale dependency study includes 6-hourly and daily model outputs from the full 4.5 years of simulations. All extreme statistics provided are “mean statistics” (time-

and zonal averaged) for extremes, and our definition of extremes leads to 210 extreme events per latitude per year when assessed at the coarse scale (240 km) using 6-hourly data; basic statistical inferences using both the mean and variability of the extremes suggest that one year of data is sufficient for statistical robustness (with $\leq 10\%$ error at a 5% significant level) because of the zonal, hemispheric, and seasonal symmetry of the aqua-planet simulations.

3. Methodology

Precipitation extremes are defined, similar to O'Gorman and Schneider (2009), as 6-hourly precipitation that exceeds the 99.9th percentile, including both wet and dry cases in a one-year simulation. Considering the large meridional variability in precipitation, extremes are determined by latitude. In the zonally symmetric aqua-planet simulations with no seasonality, stable statistics can be obtained for extreme precipitation using all 6-hourly precipitation samples from all grid points for each latitude band in both northern and southern hemisphere.

Assuming conservation of water vapor and ignoring ice formation, the moisture budget equation can be written in a vertically integrated flux form:

$$P - E = -\frac{1}{\rho_w g}\int_0^{p_s}\frac{\partial q}{\partial t}dp - \frac{1}{\rho_w g}\int_0^{p_s} u\frac{\partial q}{\partial x}dp - \frac{1}{\rho_w g}\int_0^{p_s} v\frac{\partial q}{\partial y}dp - \frac{1}{\rho_w g}\int_0^{p_s}\omega\frac{\partial q}{\partial p}dp \qquad (1)$$

The left hand side of Eq. 1 includes precipitation (P) and evaporation from the surface (E), while the right hand side consists of, from left to right, column integrations of local tendency, meridional advection of specific humidity, zonal advection of specific

humidity, and vertical advection of specific humidity. The total of the last three terms is called total advective convergence and is denoted by 'TOTDIV' in the main text. Related variables and constants are specific humidity (q), water density (ρ_w), gravitational acceleration (g), zonal velocity component (u), meridional velocity component (v), vertical velocity at pressure coordinate (omega, ω), time (t), and surface pressure (p_s). Tendency and advective terms were calculated on 20 pressure surfaces before the column integration.

For simplicity, throughout the rest of the manuscript '{ }' is used to represent the linear operator consisting of a definite integral and multiplication by a constant which is the inverse product of ρ_w and g, i.e., for any variable A,

$$\{A\} = \frac{1}{\rho_w g}\int_0^{p_s} A\, dp$$

Monthly averages are used to represent the mean fields as a common convention (e.g., Seager et al., 2012; Trenberth and Guillemot, 1995). Since seasonality is not represented in the aqua-planet simulations, annual means are used for all the large-scale means for a grid point. The transient eddy quantities are estimated as the deviations of the six-hourly values from the mean. Thus, a variable (such as ω) can be written as a mean field component ($[\omega]$) and an eddy component (ω'):

$$\omega = [\omega] + \omega'.$$

Each advective term can be further divided into an eddy term and a mean flow term. The large-scale mean is estimated for each grid box using its annual mean. The advective vertical moisture convergence term can be divided into four terms:

$$-\left\{\omega\frac{\partial q}{\partial p}\right\} = -\left\{[\omega]\frac{\partial [q]}{\partial p}\right\} - \left\{\omega'\frac{\partial q'}{\partial p}\right\} - \left\{[\omega]\frac{\partial q'}{\partial p}\right\} - \left\{\omega'\frac{\partial [q]}{\partial p}\right\} \quad (2)$$

The horizontal moisture convergence terms can be broken down into mean flow and eddies components in a similar manner.

Equation (1) is used to describe the moisture budgets for the mean conditions as well as conditions under the 99.9th percentile extremes. In the latter, the 99.9th percentile extreme events are identified based on 6-hourly precipitation data and the various terms in the equation (1) are calculated for each event before time and space averaging. Approximately 10-degree latitude bands were selected to investigate in more details the vertical characteristics of the moisture transport.

4. RESULTS and DISCUSSION

4.1 Sensitivity of extremes at native grid resolution

Here analysis is performed using model outputs at the native grid resolution of the simulations (i.e., the grid resolution at which the simulations were performed). As shown in Fig. 1, the means of the precipitation extremes show large variations with the native grid resolution and temporal resolution of the data (6-hourly, 12-hourly, daily or every 5-day) over most of the latitude ranges. The variation in extremes at the native grid resolution is much larger than that of the mean values (dashed lines in Fig. 1). Depending on the dynamical cores used, the intensities of precipitation extremes vary considerably, especially over the tropics, and the extremes from the HOMME and EUL simulations show stronger variation with resolution than those from MPAS-A at their native grid (figure not shown). It is also interesting to note that for MPAS-A, increasing grid resolution to 30 km leads to double peaks at the tropics in both mean and extreme precipitation. This feature corresponding to double Intertropical Convergence Zone

(ITCZ) has been analyzed and discussed by Landu et al. (2013) and seems to be unique to MPAS-A despite the same physics and similar grid resolutions were applied to HOMME and EUL.

Motivated by the large dependency of extremes on the native grid resolution and temporal frequency of the data, we first investigate the relative contribution of different moisture budget terms to extremes using data on the native grid from MPAS-A (Section 4.2) to provide insights on processes that are responsible for the resolution and temporal frequency dependency. Next, we explored whether the precipitation extremes converge with increasing grid resolution and the sensitivity of the results to temporal resolution when the extreme precipitation is compared at the same grid resolution using 6-hourly and daily data (Section 4.3). Both simulations with the MPAS-A and HOMME dynamical cores are included in the analysis in Section 4.3 to determine if the results are consistent among simulations with different dynamical cores. Finally, the resolution dependency of extremes is further investigated from budget analysis and the grid-scale and subgrid scale variability of vertical velocity (omega).

4.2 Moisture budget

4.2.1 Mean versus extreme conditions

Analysis of moisture budget was carried out using 6-hourly model outputs at the native grid resolution of each simulation. Averaged over the long term, the difference between mean precipitation (P) and surface evaporation (E), P-E, is roughly balanced by the divergence of the time-averaged, column integrated moisture flux in the simulated aqua-planet atmosphere (Fig. 2), which is consistent with findings by others based on

global reanalysis or global climate simulations (Trenberth and Guillemot, 1995; Seager and Vecchi, 2010). As shown in Fig. 2, the latitudinal variation and magnitudes of P-E are similar to those of the total advective convergence, although P-E is substantially more negative than TOTDIV over the subtropical regions. For the mean conditions, E is a significant term compared to P at all latitudes, and the tendency term is negligible (not shown).

During extremes, E is non-negligible but comparably small (<8% of P), so the intensity of the simulated extreme precipitation is approximately balanced by the corresponding advective moisture convergence in our aqua-planet simulations as shown in Fig. 3 for MPAS-A. The magnitudes of the advective moisture convergence typically agree with the corresponding extreme precipitation intensity within several percent. For example, in the MPAS-A simulations, the ratios of TOTDIV to P during extremes are 0.97–0.98 at 5°N-5°S and 0.95–1.0 at 25°-35° in latitude, respectively. Since the extreme defined in this study is also a measure of zonal and temporal variability, the small E compared to P during extremes suggests that the dominant spatial and temporal variability in P-E originates from P, not E, consistent with the results by Trenberth and Guillemot (1995). The typical several percent differences between P and TOTDIV indicate that the strength of the simulated precipitation extremes is approximately balanced by the corresponding total advective moisture convergence as follows,

$$P \approx -\frac{1}{\rho_w g}\int_0^{p_s} \vec{V}\cdot\nabla q\, dp - \frac{1}{\rho_w g}\int_0^{p_s} \omega \frac{\partial q}{\partial p}\, dp \qquad (3)$$

Thus, the resolution dependency in precipitation extreme could be investigated from the scale dependency of the advective moisture convergence. All analyses described below

focus on the contributions of different moisture budget terms to precipitation extremes based on the aqua-planet simulations with the MPAS-A dynamical core.

4.2.2 Horizontal versus vertical advection

It is worth noting that the horizontal advective moisture convergence is very small (≤2% of total moisture convergence) compared to its vertical counterpart over the tropics, suggesting that the total advective convergence can be approximated by the vertical moisture transport, $\{-\omega\delta q/\delta p\}$, over this region (Fig. 3). However, the same rule does not apply over the extra-tropics, where horizontal advective moisture convergence contributes up to ~20% of TOTDIV. Zonal advective convergence, $\{-u\delta q/\delta x\}$, is negligible at most latitude ranges except near ~30° in latitude, where negative values indicating local drying associated with the subtropical high pressure system are important, with magnitudes of roughly several percent (~7–10%) of TOTDIV with MPAS-A.

The relative importance of moisture transport at zonal, meridional, and vertical directions and their variations with the native grid resolution at different vertical layers are illustrated for two selected latitudinal bands (Fig. 4). A 5°S–5°N band represents the tropical region where only vertical moisture transport is important, and the 25°–35° band (including both hemispheres) represents the extratropical regions where zonal, meridional, and vertical moisture advective transport are all non-negligible. Consistent with the previous results, the moisture transport over both latitude bands is dominated by the vertical moisture transport (Fig. 4), which shows a strong sensitivity to the model's native grid resolution. The vertical moisture transport peaks at the mid-atmosphere (~600

hPa and ~700 hPa for the tropical and subtropical bands, respectively) where its sensitivity to the native grid resolution is also the largest. Zonal and meridional transport is negligible over the tropics, but over the extra-tropical band, zonal and meridional transport also plays a role especially in the lower atmosphere. Over this region, zonal moisture transport ($-u\delta q/\delta x$) contributes to drying of the atmosphere below ~650 hPa, and this term increases slightly in magnitude with increasing native grid resolution below ~800 hPa. The meridional moisture transport over the extra-tropical band has magnitudes comparable to the vertical moisture transport near the surface layer (P_a > 900 hPa) but decreases with height and becomes fairly small above 400 hPa. The meridional transport ($-v\delta q/\delta y$) over this region shows a slight converging tendency with similar values at high resolution. Over both tropical and extra-tropical bands, the variation of TOTDIV during extremes with the native grid resolution is dominated by the corresponding variation in vertical moisture transport that maximizes in the mid-troposphere where the dependency on the native grid resolution is also the greatest.

4.2.3 Mean fields versus transient eddies

The vertical advective convergence is further partitioned into mean fields and transient eddy components according to Eq. 2 (Fig. 5 for MPAS-A) to estimate the relative contributions of mean circulation and eddies to extremes. Over both tropics and extra-tropics, the eddy transport of mean moisture, $\{-\omega'\delta[q]/\delta p\}$, is the dominant term, followed by eddy transport of eddy moisture, $\{-\omega'\delta q'/\delta p\}$. While these two terms are comparable in magnitude over the extra-tropics (e.g., 76.4 vs. 53.5 mm day^{-1} over 30–35°N at 30 km with MPAS-A), the former is several times higher (e.g., 377.8 vs. 76.4

mm day^{-1} over 5°S–5°N at 30km resolution with MPAS-A) than the latter over the tropics. The mean flow term {-[ω]δ[q]/δp} is not significant (< 0.8 mm day^{-1} with MPAS-A) at all latitudes except over a narrow band centered at the equator where it shows converging tendency with increasing native grid resolution in MPAS-A (11.5, 13.5, 14.4, 14.5 mm day^{-1} for 240, 120, 60, and 30 km). The third term of Eq. 2 ({-[ω]δq'/δp}) is negligible (<0.05 mm day^{-1} over tropics and extra-tropics). Thus, the large variation of the vertical advective moisture transport at the native grid resolution is mainly coming from that of the two eddy terms, {-ω'δ[q]/δp} and {-ω'δq'/δp}.

Similar breakdowns of zonal and meridional advective convergence found that zonal mean flow transport of eddy moisture, {-[u]δq'/δx}, and meridional eddy transport of eddy moisture, {-v'δq'/δy}, are only significant over the extra-tropical subtropical band during extremes where {-[u]δq'/δx} slightly dries the storm at most vertical levels, while {-v'δq'/δy} along with vertical moisture transport supply moisture for the extreme precipitation over this region. In the lower atmosphere (*p* >~850 hPa), the vertical eddy transport of eddy moisture, -ω'δq'/δp, contributes negatively to P during extremes over both tropics and extra-tropics. Although both instantaneous (q) and large scale [q] specific humidity decreases with height, the eddy moisture (q') peaks at around 850-875 hPa vertically (figure not shown). This is likely to result from low-level convergence, especially that at the zonal direction, which brings drier and colder air from the outer region to the convective center. As a result of the reverse vertical gradients of eddy moisture (q') and the strong upward eddy motion, -ω'δq'/δp dries the lower level and contributes negatively to precipitation intensity during extremes. Over the tropics, the source of moisture, its associated energy, and the resolution dependency of the moisture

transport at the native grid resolution are dominated by eddy transport of mean moisture (-ω'δ[q]/δp). However, over the extra-tropics, this is true only for the lower altitudes ($p >$ ~700 hPa) while at higher altitudes ($p <$ ~700 hPa), the resolution dependency in the moisture transport is dominated by the eddy transport of eddy moisture (-ω'δq'/δp). At the mid-layer (~700 hPa < p < ~800 hPa) both eddy terms are comparable in terms of their contributions to the total moisture convergence and its resolution dependency.

On examining the moisture and omega profiles (not shown), it is indicated that the resolution dependency of omega assessed at the native grid resolution is large, which passes on to the vertical moisture transport terms; the vertical moisture structures in mean and eddies quantities act as an averaging kernel, which determines the relative contribution of the resolution dependency and magnitude of omega at different levels to the scale dependency and magnitude of the column integrated moisture transport assessed at the native grid resolution. Over the tropics, the mean atmosphere is already very humid (~13 g kg^{-1} near surface), and [q] decreases very sharply with the increasing altitude. As a result, the vertical gradients of *[q]* are much larger than that of *q'*, which in addition to the more significant drying at the lower atmosphere associated with the reverse vertical moisture gradients results in larger magnitude and larger resolution dependency of {-ω'δ[q]/δp} than {-ω'δq'/δp} over the tropics. Over the extra-tropics, however, the mean atmosphere above ~700 hPa is much drier and has a small vertical gradient compared to that under extreme conditions, which explains the dominance of {-ω'δq'/δp} over {-ω'δ[q]/δp} in magnitudes and dependency on the native grid resolution for the upper atmosphere over this region.

4.2.4 Dynamics versus thermodynamics

Previous analysis has identified the relative role of mean circulation and eddies in the moisture transport and characterized their variation with the native grid resolution at different vertical layers under extreme conditions. An important question to ask is how much of the variation with the native grid resolution is due to changes in dynamics versus thermodynamics. The dependency on the native grid resolution is represented by the difference, 'Δ', between the fine resolution and coarse resolution (240 km for MPAS-A) simulations. The resolution dependency of moisture transport is estimated as follows:

$$\Delta\left(\omega\frac{\delta q}{\delta p}\right) = \Delta(\omega)\frac{\delta q}{\delta p} + \omega\Delta\left(\frac{\delta q}{\delta p}\right) + \Delta(\omega)\Delta\left(\frac{\delta q}{\delta p}\right) \quad (4),$$

where the three terms on the right-hand side represent changes due to dynamic (ω), thermodynamic (q), and covariance changes. Note that for simplicity, the negative sign is ignored in the vertical moisture transport term in Eq. 4. As shown in Fig. 7, the profiles of $\Delta(\omega\delta q/\delta p)$ and $\Delta(\omega)\delta q/\delta p$ under extreme conditions are close to each other with typical agreement within 10% in magnitude at most vertical layers. This indicates that the variation of vertical moisture transport with the native grid resolution is mainly explained by the changes in dynamics (ω) with native grid resolution at most altitude ranges.

4.3 Scale dependency at the same grid scale

Because coarse simulations cannot produce the fine scale features resolvable by the higher resolution simulations, a more useful analysis of resolution dependency is to compare simulations aggregated to the same spatial resolution. For such an analysis, the resolution dependency is represented by the difference, 'Δ', between the fine and coarse resolution simulations after the fine resolution simulations have been aggregated or

upscaled to the coarse resolution grid using area-weighted averaging. We define convergence as the time-averaged, zonal mean of extremes in simulations performed at different grid resolutions but aggregated to the same coarse resolution are not statistically different (at a 5% significance level) from each other. That is, simulations performed at a range of grid resolutions do not exhibit a resolution dependency when they are aggregated to the same grid resolution for comparison. Fig. 8 shows the zonal averaged mean and extreme precipitation for simulations performed at 30 km, 60 km, 120 km, and 240 km grid resolution, all compared at the 240km grid resolution for MPAS-A, and similarly for HOMME. Interestingly, the double ITCZ feature simulated at 30 km resolution simulation with MPAS-A disappears or becomes inconspicuous after upscaling to the coarse grid, which indicates the association of this feature with small-scale variability. Neither the mean nor extreme precipitation shows convergence over the tropics and the differences between high and low resolution simulations do not vary monotonically with grid resolution. This is seen more clearly for extremes in Fig. 9 that shows the difference, 'Δ', between higher resolution simulations aggregated to 240 km grid resolution and the coarse resolution simulation performed at 240 km grid resolution. There is no convergence of extremes over the tropics (i.e., 'Δ' is statistically different from zero) in MPAS-A at 6-hourly and daily time scales. The same is true when assessed at 120 km or 60 km grid scales for the MPAS-A simulations using 6 hourly, 12 hourly, or daily data (not shown). Similarly, simulations with HOMME do not converge at 6-hourly or daily time scales over the tropics.

Over the extra-tropics, for both dynamical cores, Fig. 9 shows that the simulations do not converge when compared at the coarse grid scale except for a small latitude range

(~20-25°) for MPAS-A. The magnitudes of extremes from the coarse resolution simulations (blue lines in Fig. 8) are much lower than that from the finer grid resolutions, and there is a poleward shift of the extra-tropical peak (~30° in latitude) from coarse to fine resolutions. The poleward shift is even more apparent when the simulations are compared at their native grid resolution (Fig. 1). The scale dependency is reduced when coarser temporal resolution data are used over the extra-tropical regions. As shown in Fig. 9, at daily time scale, the differences between high and low resolution simulations become negligible so the four simulations performed at grid resolutions ranging from 30 to 240 km essentially converged at a wide range of latitudes (e.g., 50-65° for MPAS-A). When assessed at the 120 km scale using 6 hourly data, simulations at 60 and 30 km resolution with the MPAS-A converge over 20-50° in latitude (Figure not shown). When assessed at the 120 km scale using daily data, simulations with MPAS-A converge in the latitude range of 15-60° (figure not shown). The scale dependency of simulations with HOMME over the extra-tropics region is similar but generally larger than that with MPAS-A (Fig. 9). There is no converging tendency over the high latitudes (>70°) for simulations with both dynamical cores. We note, however, that near the poles, sampling becomes an issue as the number of grid cells becomes much smaller.

The dynamical and thermodynamical contributions to the scale dependency of extremes compared at the same grid scale are shown in Fig. 10 for the tropical and extra-tropical bands. The contributions from thermodynamic changes are generally consistent between MPAS-A and HOMME. When assessed at the same coarse grid scale, thermodynamic (moisture) changes become significant in offsetting the dynamic effect (omega), especially over the extra-tropics, although contributions from dynamic changes

to the scale dependency is still larger and explain most of the scale dependency of the vertical advective moisture convergence. Contributions of thermodynamic changes are negative within most vertical layers over both tropics and extra-tropics for both dynamical cores, thus reducing the overall scale dependency. The offsetting thermodynamic effects are associated with the decrease in specific humidity with resolution for both mean and extreme conditions with either dynamical core. The contributions of dynamic changes to scale dependency are positive except over the tropics for MPAS-A where their contributions are negative.

Over the tropics, with the MPAS-A dynamical core, both dynamical changes and thermodynamical changes become more negative with increasing resolution (panel a of Fig. 10), so the extremes do not converge. Although thermodynamical changes offsets some of the scale dependency caused by the dynamics with HOMME over the tropics, the scale dependency from dynamics contributions is several times larger in magnitude than that over the extra-tropics (note the different scales used in the x-axis for panels c and d). The scale dependency remains too large for the simulations to converge even when assessed using daily data.

At the upper atmosphere (< ~300 hPa) in the 58km simulation with HOMME, the resolution dependency is mainly explained by changes in thermodynamics over both latitudinal bands, which is an exception. This is likely due to the higher convective cloud tops simulated at 58 km resolution with HOMME. A slightly more humid atmosphere (especially above ~700 hPa) is seen in the 58 km simulation with HOMME under both mean and extreme conditions and the more humid atmosphere allows storms to reach higher tops. The differences in thermodynamics in the HOMME simulations at the upper

atmosphere are likely influenced by non-linear feedbacks from large changes in dynamics, which require further investigation.

The dominant contributions of dynamics changes to scale dependency of the vertical moisture transport during extremes warrant further examination of the sensitivity of omega with resolution. As indicated by the vertical velocity spectra in Lean and Clark (2003), the vertical velocity in a convective system consists of variability at scales much smaller than the finest grid spacing used in our experiments. When upscaled to coarse grid scale through averaging, signals/variances at scales smaller than the analysis scale are reduced at coarser resolution, so mismatch of process and analysis scales often leads to difficulty in producing reliable statistics from aggregating areal data (McComiskey and Feingold, 2012). While data aggregation does not alter the mean values, it does impact extreme intensities since extremes represent events with high temporal and spatial variability.

The differences in omega in the fine (ω_{fine_n}) and coarse (ω_{coarse_n}) simulations at their respective native grid resolution can be expressed as a sub-grid scale (SGS) component not resolvable by the coarse simulation, and the difference between the simulations when compared at the same grid scale (ΔGS):

$$\omega_{p,fine_n} - \omega_{p,coarse_n} = SGS + \Delta GS$$

$$SGS = \omega_{p,fine_n} - \omega_{p,fine2coarse}$$

$$\Delta GS = \omega_{p,fine2coarse} - \omega_{p,coarse_n} \qquad (5)$$

where the sub-grid variability can be estimated as the difference between the statistics of the simulations aggregated to the coarse scale (denoted as ‘fine2coarse’ in the subscript) and simulations at the native grid resolution (denoted by ‘fine_n’ in the subscript). This

approach of estimating sub-grid scale variability is a variation of the approach used by Cheng et al. (2010) and Mason and Brown (1999), in which a running mean operator on both horizontal directions was used. Note that although the negative sign is not indicated, 'p' refers to the 99.9th percentile of negative omega (equivalent to 0.1th percentile of omega) for consistency with the use of high percentiles in the precipitation extreme definition. As an example, $\omega_{p,30to240}$ denotes the 99.9th percentile of the negative omega (upward motion) that has been aggregated (area-weighted averaged) from the 30 km native grid resolution to the 240 km coarse grid scale, and it represents the resolved 240 km grid-scale variability of the fine resolution simulation. Thus, SGS and ΔGS for fine-resolution simulation (30km) at 240 km grid scale is expressed as below:

$$SGS = \omega_{p,30_n} - \omega_{p,30to240}$$

$$\Delta GS = \omega_{p,30to240} - \omega_{p,240_n}$$

The difference ΔGS is the difference between fine (e.g., 30 km) and coarse (e.g., 240 km) simulations after aggregating the fine resolution (e.g., 30km) to the coarse (e.g., 240 km) grid scale. When assessing the scale dependency at the native grids, SGS dominates, but when assessing the scale dependency at the same grid scale, the difference is smaller as ΔGS is generally much smaller than SGS.

The probability density functions (PDFs) of the simulated ω at their native grid (e.g., the red dashed, green dotted, and blue solid curves in Fig. 11 corresponding to PDFs of ω from simulations performed at 60/58 km, 120/110 km, and 240/220 km, respectively) become increasingly broader accompanied by more extreme tail values with the increase in native grid resolution. The differences of PDFs at the same coarse grid scale (e.g., ω_{30to60}(black dashed) versus ω_{60_n} (red dashed) in panels a and c of Fig.11

for MPAS-A in the tropics and extra-tropics, respectively) are relatively small. This indicates that the resolution dependency of the extreme vertical velocity at the native grid resolution can be largely explained by the SGS variability, although the contributions from ΔGS are not negligible.

Following the above analysis, the sensitivity of extreme vertical velocity to spatial grid spacing is illustrated quantitatively in Fig. 12, along with those of the mean vertical velocity. With both MPAS-A and HOMME, the mean negative omega at 600 hPa are positive (upward) and in general increases with increasing resolution over both tropical and extra-tropics bands and show monotonic converging tendency over extra-tropical regions.

The sensitivity of extreme vertical velocity to resolution is different from that of the means. The 99.9th percentiles of the negative omega (ω_p) at the native grid resolution increase drastically and almost linearly as the resolution doubles (not shown), but this scale dependency of omega at the native grid resolution is dominated by the SGS variability, as inferred from Fig. 11. Differences in ω_p when compared at the same grid scale (ΔGS) (e.g., $\omega_{p,60_n} - \omega_{p,30to60}$) indicate the resolution dependency after accounting for the sub-grid scale variability resolved by increasing resolution. The ΔGS, although small, explains the scale dependency of vertical moisture transport simulated at different resolutions but compared at the same grid scale (Fig. 10). At 600 hPa, the vertical level with maximum of scale dependency from Fig. 10, the increasingly negative ΔGS with increasing resolution (solid line on panel b of Fig. 12) explains the non-convergence of vertical moisture transport over the tropics with MPAS-A. Note that the unique negative ΔGS in MPAS-A is likely associated with the unique double ITCZ

feature in the fine resolution simulation and they are likely to share the same causes. Over the extratropical band, there are some reductions of ΔGS with increasing resolution (e.g., solid line on panel e of Fig. 12) with MPAS-A, and the magnitude of ΔGS is small enough to allow convergence at certain grid scale using either 6-hourly or daily data (e.g., 60 km grid scale with 6-hourly data and 240 km grid scale with daily data). This is consistent with the previous analysis of MPAS-A that over the extra-tropics, thermodynamic (moisture) changes become significant in offsetting the scale dependency due to dynamics (omega), which leads to the convergence at certain grid scale using daily or 6-hourly data. For both tropical and extratropical bands, the magnitudes of ΔGS are several times larger with HOMME compared with MPAS-A. The relatively large ΔGS in HOMME (note the difference in scale in the y-axis) translates to larger scale dependency in vertical moisture transport than MPAS-A. The generally positive ΔGS (except over the tropics with MPAS-A) indicates that the effects of sub-grid scale variability at the grid scales must be adequately parameterized in the model at coarse resolution to improve "scalability" or consistency in extreme vertical velocity when assessed at the same grid scale.

The intensities of precipitation extremes and the corresponding high percentile vertical motions are much higher in HOMME than MPAS-A over the tropics. This could be explained partly by the 20% higher effective resolution with HOMME compared to MPAS-A at similar grid resolution (figure not shown). Comparison of the kinetic energy spectra from MPAS-A and HOMME reveals that MPAS-A is slightly more dissipative than HOMME (figure not shown); however the differences are relatively small and unlikely to be the main reason for the large differences from MPAS-A regarding extreme

precipitation over the tropics. A one-year HOMME test run replacing the vertical discretization approach from Simmon and Burridge (1982) used in the HOMME simulations analyzed in this study by the vertical Lagrangian method reduces the mean precipitation simulated by 15% near the equator, which brings the HOMME simulations closer to MPAS-A in terms of the mean precipitation values over the tropics. However, changing the vertical discretization approach in HOMME appears to have little impacts on the extreme precipitation. Further investigation is required to identify the main reason leading to the large differences between HOMME and MPAS-A simulations when the same CAM4 physics package is used.

5. SUMMARY and CONCLUSIONS

In this study, we examine the resolution dependency of precipitation extremes in climate models. This has implications for projecting changes in climate variability and extremes in the future. A set of aqua-planet simulations produced by a global model using the same physics parameterizations but different dynamical cores and horizontal grid resolutions were used in this investigation. Strong increases of precipitation extremes with native grid resolutions are seen over both tropics and extra-tropics. The magnitude of this dependency also varies with dynamical cores, especially over the tropics. Moisture budget estimates based on the aqua-planet simulations with MPAS-A suggest that during precipitation extremes, surface precipitation is approximately balanced by the advective moisture convergence with evaporation contributing an insignificant amount; although evaporation plays a much larger role in providing moisture for the mean precipitation. This is particularly true over the tropics, where the vertical advection of moisture

explains nearly all of the surface precipitation during precipitation extremes. Over the extra-tropics where the contribution of vertical moisture transport still dominates the total moisture transport, meridional advection also contributes.

The variation of moisture transport with the native grid resolution is mainly due to the eddy transport of mean moisture {-ω'δ[q]/δp} and the eddy transport of eddy moisture {-ω'δq'/δp}. At most vertical levels over the tropics and in the lower atmosphere over the extra-tropics, the interaction between eddies and mean moisture field, {-ω'δ[q]/δp}, dominates the contribution to precipitation extremes. Over the extra-tropics, the source of moisture and its associated energy are dominated by eddy transport {-ω'δq'/δp} at the mid- and upper-troposphere. With either MPAS-A or HOMME dynamical core, the resolution dependency of the vertical advective moisture convergence during extremes is mainly explained by dynamical changes (related to omega). Although the vertical gradients of moisture act like averaging kernels that determines the relative contributions of the changes in omega at different vertical levels to the overall scale dependency. The scale dependency of extremes is also assessed by aggregating (using area-weighted averages) the fine resolution simulations to the coarse resolution grids for comparison. The extreme precipitation does not converge with resolution over the tropics for simulations with either MPAS-A or HOMME when all simulations are compared at 240/220 km (and also at finer grid scales) with either 6 hourly or daily data. Over the extra-tropics, extremes in simulations with both dynamical cores do not converge at the coarse grid scale (240 km for MPAS-A and 220 km for HOMME) at most latitudes. However, the scale dependency is reduced when coarser temporal resolution data are used, and convergence in extreme is found with daily data

over a wide range of latitudes in the extra-tropics. In addition, there is a poleward shift in extra-tropical peak of extreme precipitation (~30° in latitude) from coarse to fine resolutions, which is very clear when comparing simulations at their native grid resolution, and still apparent even when comparing simulations that are aggregated to the coarse scale.

When assessed at the same grid scale through aggregation of the finer resolution simulations, thermodynamic (moisture) changes become significant in offsetting the effect of dynamics (omega), especially over the extra-tropics, although dynamics still show a more dominant impact on the resolution dependency than thermodynamics over most vertical layers, especially in the mid-troposphere where the resolution dependency in vertical moisture transport is the largest.

This study shows that extreme precipitation in aqua-planet simulations by the Community Atmosphere Model (CAM) demonstrates spatial resolution and dynamical core dependency, especially over the tropics, despite the fact that the same physics parameterizations were used. Simulations with the HOMME dynamical core shows higher variability in the vertical motion, leading to higher extreme precipitation intensities and a resolution dependency beyond what can be explained by a 20% higher effective resolution in HOMME compared to MPAS-A, which requires further investigation. Differences in simulations compared at the same grid scale suggest that the effects of sub-grid variability in omega and vertical moisture transport during extreme conditions are not adequately parameterized at coarse resolutions in both MPAS-A and HOMME and more so for the latter.

Li et al. (2011a) have also identified omega as the source of resolution dependency of extreme precipitation in aqua-planet simulations using simple correlation coefficients to attribute the likely causes. This study quantifies the relationship between omega and extreme precipitation using detailed moisture budget equation, with an added focus on comparing how the relationship varies with dynamical cores. Sugiyama et al. (2010) showed that changes of PE under global warming are strongly linked to the magnitude and profile of vertical velocity in the tropics. GCM projections of future PEs have been found to be very sensitive to model resolution and parameterizations (O'Gorman and Schneider 2009). Hence the resolution and dynamical core dependency of extreme precipitation has important implications to the prediction of future changes in extreme precipitation.

Williamson (2008) discussed the behavior of extreme precipitation in the equatorial region (10°S-10°N) in the form of the probability density function using simulations with the CAM Finite Volume dynamical core. Our analysis extends his study by including results from different dynamical cores. In light of the sensitivity of extreme precipitation and vertical velocity to dynamical cores, in addition to model resolution, future studies should further investigate how dynamical cores interact with model resolution and physics parameterization to influence extreme precipitation. Future development in convective parameterizations needs to address not only spatial-resolution dependency but also dynamical core dependency. Convective parameterizations that incorporate probability density functions of omega might better capture the variability of vertical motion during extremes and improve consistency of extreme precipitation intensity simulated with different dynamical cores at different spatial resolution. The

aqua-planet framework and analysis described in this study provide an important metric for assessing the sensitivity of cloud parameterizations to spatial resolution as well as dynamical cores under extreme conditions.

Acknowledgements:

We would like to thank Samson Hagos and Kiranmayi Landu for the helpful discussion and the internal review of this manuscript. This research was supported by the Office of Science of the U.S. Department of Energy as part of the Regional and Global Climate Modeling program. The Pacific Northwest National Laboratory is operated for DOE by Battelle Memorial Institute under contract DE-AC05-76RL01830.

Reference:

Allan, R. P. and B. J. Soden, 2008: Atmospheric warming and the amplification of precipitation extremes. Science, 321, 1481-1484.

Arakawa, A., J.-H. Jung, and C.-M. Wu, 2011: Toward unification of the multiscale modelling of the atmosphere. *Atmos. Chem. Phys.*, **11**, 3731-3742, doi:10.5194/acp-11-3731-2011.

Berg, P., C. Moseley, and J. O. Haerter, 2013: Strong increase in convective precipitation in response to higher temperatures. *Nature Geosci.*, **6**, 181-185, doi:10.1038/NGEO1731.

Boyle, J. and S. Klein, 2010: Impact of horizontal resolution on climate model forecasts of tropical precipitation and diabatic heating for the TWP ICE period. *J. Geophys. Res.*, **115**, D23113, doi:10.1029/2010JD014262.

Buizza, R., 2010: Horizontal resolution impact on short and long-range forecast error. *Q. J. ROY. Meteorol. Soc.*, **136**, 1020–1035.

Cheng, A., K.-M. Xu, and B. Stevens, 2010: Effects of resolution on the simulation of boundary-layer clouds and the partition of kenetic energy to subgrid scales, *J. Adv. Model. Earth Syst.* **2**, 21pp, doi:10.3894/JAMES.2010.2.3.

Coumou, C. and S. Rahmstorf, 2012: A decade of weather extremes. *Nature Geosci.*, **2**, 491-496, doi:10.1038/NCLIMATE1452.

Evans et al., 2013: *AMIP Simulation with the CAM4 Spectral Element Dynamical Core*, J. Climate, **26**, 689-709.

Hack JJ. 1994: Parameterization of moist convection in the National Center for Atmospheric Research Community Climate Model (CCM2). *J. Geophys. Res.*, **99**:

5551–5568.

Held, I. M. and B. J. Soden, 2006: Robust responses of the hydrological cycle to global warming. *J. Climate*, **19**, 5686-5699.

Landu, K., L.R. Leung, S. Hagos, V. Vinoj, S. A. Rauscher, T. Ringler, and M. Taylor, 2013: The dependence of ITCZ structure on model resolution and dynamical core in aqua-planet simulations. *J. Climate*, submitted.

Lean, H. W. and P. A. Clark, 2003: The effects of changing resolution on mesoscale modelling of line convection and slantwise circulations in FASTEX IOP16. *Quart, J. Roy. Meteor. Soc.*, **129**, 2255-2278.

Leung L. R., T. Ringler, W. D. Collins, M. Taylor, and M. Ashfaq. 2013: A Hierarchical Evaluation of Regional Climate Simulations." *Eos* **94**, 297-298, doi:10.1002/2013EO340001.

Li F., W. D. Collins, M. F. Wehner, D. L. Williamson, J. G.Olson, and C. Algieri, 2011: Impact of horizontal resolution on simulation of precipitation extremes in an aqua-planet version of Community Atmospheric Model (CAM3). *Tellus*, **63A**, 884-892.

Li F., W. D. Collins, M. F. Wehner, D. L. Williamson, and J. G. Olson, 2011: Response of precipitation extremes to idealized global warming in an aqua-planet climate model: towards a robust projection across different horizontal resolutions. *Tellus*, **63A**, 876-883.

Mason, P. J. and A. R. Brown, 1999: On subgrid models and filter operations in large eddy simulations. *J. Atmos. Sci*, **56**, 2101-2114.

McComiskey A. and G. Feingold, 2012: The scale problem in quantifying aerosol indirect effects, *Atmos. Chem. Phys.*, 12, 1031-1049, doi:10.5194/acp-12-1031-2012.

Mishra, S. K., M. A. Taylor, R. D. Nair, P. H. Lauritzen, H. M. Tufo, and J. J. Tribbia, 2011: Evaluation of the HOMME dynamical core in the aquaplanet configuration of NCAR CAM4: Rainfall. *J. Climate*, **24**, 4037–4055.

Neale, R. B. and B. J. Hoskins, 2000: A standard test for AGCMs including their physical parametrizations: I: The proposal. *Atmos. Sci. Lett.*, **1**, 101-107.

Neal, R. B. et al., 2010: Description of the NCAR Community Atmosphere Model (CAM 4.0). Tech. Rep. NCAR/TN-485+STR, NCAR.

O'Gorman, P.A., and T. Schneider, 2009: The physical basis for increases in precipitation extremes in simulations of 21st – century climate change. *PNAS*, **106**, 14773-14777.

Paul A. O'Gorman, Tapio Schneider, 2009: Scaling of Precipitation Extremes over a Wide Range of Climates Simulated with an Idealized GCM. *J. Climate*, **22**, 5676-5685.

Randall, D. A., Wood, R. A., Bony, S., Colman, R., Fichefet, T. and co-authors. 2007. Climate models and their evaluation. In: Climate Change, 2007: The Physical Science Basis. Contribution of Working Group I to the Fourth Assessment Report of the Intergovernmental Panel on Climate Change. (eds. Solomon, S., D. Qin, M. Manning, Z. Chen, M. Marquis, K. B. Avery, M. Tignor and H. L. Miller). Cambridge University Press, Cambridge, United Kingdom and New York, NY, USA.

Rasch, P. J., and J. E. Kristjánsson, 1998: A comparison of the CCM3 model climate using diagnosed and predicted condensate parametrizations. *J. Climate*, **11**, 1587–1614.

Rauscher, S. A., T. D. Ringler, W. C. Skamarock, and A. A. Mirin, 2013: Exploring a Global Multiresolution Modeling Approach Using Aquaplanet Simulations. *J.*

Climate, **26**, 2432-2452, doi:10.1175/JCLI-D-12-00154.1.

Seager, R., and G. A. Vecchi, 2010: Greenhouse warming and the 21st century hydroclimate of southwestern North America. *PNAS*, **107**, 21277-21282.

Stephens, GL, T L'Ecuyer, R Forbes, A Gettelmen, J-C Golaz, A Bodas-Salcedo, K Suzuki, P Gabriel, and J Haynes. 2010: Dreary state of precipitation in global models. *J. Geophys. Res.*, **115**, D24211, doi:10.1029/2010JD014532.

Sugiyama, M., H. Shiogama, and S. Emori, 2010: Precipitation extreme changes exceeding moisture content increases in MIROC and IPCC climate models. *PNAS*, **107**, No. 2, 571-575.

Taylor, M. A. and A. Fournier, 2010: A compatible and conservative spectral finite element method on unstructured grids. *J. Comput. Phys.* **229**, 5879-5895.

Trenberth, K. E., and C. J. Guillemot, 1995: Evaluation of the global atmospheric moisture budget as seen from analysis. *J. Climate*, **8**, 2255-2272.

Williamson, D. L., 1999: Convergence of atmospheric simulations with increasing horizontal resolution and fixed forcing scales. *Tellus*, 51A, 663-673.

Williamson, D. L., 2008: Convergence of aqua-planet simulations with increasing resolution in the Community Atmospheric Model, Version 3. *Tellus*, **60A**, 848-862.

Williamson, D. L., 2013: The effect of time steps and time-scales on parametrization suites, *Q. J. R. Meteorol. Soc.*, **139**, 548-560.

Zhang, G. J. and N. A. McFarlane, 1995: Role of convective-scale momentum transport in climate simulation. *J. Geophy. Res.*, **100**, 1417–1426.

Figure captions

Figure 1: Latitudinal variations of mean and extreme ($\geq 99.9^{th}$ percentile of both wet and dry conditions) precipitation with the native grid resolution (panel a) and with different temporal data frequencies (6 hourly, 12 hourly, 24 hourly, and every 5 day) for the simulation at 240 km grid resolution (panel b). Due to the relatively small magnitudes, the mean values are scaled by a factor of 5 (Mean x 5; long dashed).

Figure 2: Meridional variations of mean moisture budget terms based on simulations using the MPAS-A dynamical core with 240, 120, 60, and 30 km native grid resolution (panels a, b, c, and d, respectively). The moisture budget terms include precipitation (P, black dashed), surface evaporation (E, yellow dashed), advective moisture convergence (div, blue solid), and P-E (purple, solid).

Figure 3: Meridional variations of moisture budget terms under extreme precipitation conditions based on simulations with the MPAS-A dynamical core and with 240 km, 120 km, 60km, and 30 km horizontal grid resolutions (panels a-d), respectively. Zonal, meridional and vertical advective moisture convergence during extremes, $\{-u\delta q/\delta x\}$, $\{-v\delta q/\delta y\}$, and $\{-\omega\delta q/\delta p\}$, are shown in solid brown, blue, and green lines along with the corresponding total advective moisture convergence (sum, yellow solid) and extreme precipitation (P, black dashed).

Figure 4: Vertical profiles of zonal ($-u\delta q/\delta x$, brown), meridional ($-v\delta q/\delta y$, blue), and vertical ($-\omega\delta q/\delta p$, green) advective moisture convergence for simulations at their native

grid resolutions of 30 (dash dot dot), 60 (dotted), 120 (dashed), and 240 km (solid) with the MPAS-A dynamical core for latitude bands of 5°S–5°N (left) and 25°–35° in both hemisphere (right).

Figure 5: The breakdown of vertical advective moisture convergence during extremes into corresponding mean flow, $\{-[\omega]\delta[q]/\delta p\}$ (brown solid), and two eddies related terms, $\{-\omega'\delta q'/\delta p\}$ (yellow dotted) and $\{-\omega'\delta[q]/\delta p\}$ (green dashed), for the MPAS-A simulations at four native grid resolutions of 240, 120, 60, and 30 km. The total vertical advective moisture convergence (sum) and precipitation (P) during extremes are also shown as black dashed and dotted lines, respectively.

Figure 6: Vertical profiles of mean flow and eddy moisture transport for simulations at the native grid resolutions of 30 (dash dot), 60 (dotted), 120 (dashed), and 240 km (solid) with the MPAS-A dynamical core for the latitude bands of 5°S–5°N (Panel a) and 25°–35° (including both hemispheres, Panel b). The mean flow and eddies terms are too small and are omitted.

Figure 7: Estimated differences in vertical advective convergence ($\Delta(\omega\delta q/\delta p)$, green) between simulations at fine resolutions (30, 60, and 120 km) and that at the coarse resolution (240 km) during extremes, and the contributions to these differences by changes in dynamics ($\Delta(\omega)\ \delta q/\delta p$, blue), thermodynamics ($\omega\Delta(\delta q/\delta p)$, yellow), and their covariance changes ($\Delta(\omega)\Delta(\delta q/\delta p)$, black) relative to the coarse resolution (240 km). The estimates in this figure are based on simulations with the MPAS-A dynamical core and at their native grid resolution.

Figure 8: Variations of mean and extreme precipitation with grid resolution assessed at the same grid scale for simulations with the MPAS-A (Panel a) and HOMME dynamical cores (Panel b). The simulations conducted at fine resolutions have been aggregated (area-weighted averaged) to the coarse resolution grids (240 km for MPAS-A and 220 km for HOMME). The mean values are scaled by a factor of 5 (Mean x 5; long dashed) due to their relatively small magnitudes.

Figure 9: Differences of extreme precipitation between fine (120, 60 and 30 km for MPAS-A and 110, 55, and 28 km for HOMME) and coarse resolutions (240 km for MPAS-A and 220 km for HOMME) when assessed at the same grid using both 6 hourly (Panels a and c) and daily data (Panels b and d). The simulations conducted at fine resolutions have been aggregated (area-weighted averaged) to the coarse resolution grids (240 km for MPAS-A and 220 km for HOMME) before calculating the differences. The grey area indicates the 95% confidence interval within which the two fine resolution simulations are not statistically different.

Figure 10: Contributions of dynamics ($\Delta(\omega)\delta q/\delta p$, blue), thermodynamics ($\omega\Delta(\delta q/\delta p)$, yellow), and their covariance changes ($\Delta(\omega)\Delta(\delta q/\delta p)$, black) to the scale dependency of vertical advective convergence ($\Delta(\omega\delta q/\delta p)$, green) for simulations with the MPAS-A (Panels a and b) and HOMME dynamical cores (Panels c and d). The changes are estimated as differences relative to the coarse resolution (240 km for MPAS-A and 220 km for HOMME) at the same grid scale.

Figure 11: Resolution dependency of PDFs of -1*omega (on 600 hPa) for the 5°S–5°N (a, b) and 25°–35° (include both hemispheres) latitude bands (c, d). Colors indicate the native grid resolution the simulations were conducted. In the PDF, the different line styles indicate the coarse grid scale to which the fine resolution simulations have been aggregated, and the corresponding vertical line indicates the 99.9th percentile of the negative omega.

Figure 12: Mean negative omega (a and d) and the same grid differences (ΔGS) in 99.9th percentile of negative omega (b, c, e, and f) on 600 hPa for 5°S–5°N (top) and 25°–35° (include both hemispheres, bottom) latitude bands based on simulations with the MPAS-A or HOMME dynamical cores. The x-axis indicates the native grid resolution the simulations were conducted, and the solid line, dashed lines, and filled circle indicate the grid scales (240, 120, and 60 km for MPAS, respectively, and 220,110, and 55 km for HOMME, respectively) the fine resolution simulations were aggregated to for the grid scale comparison.

Figures

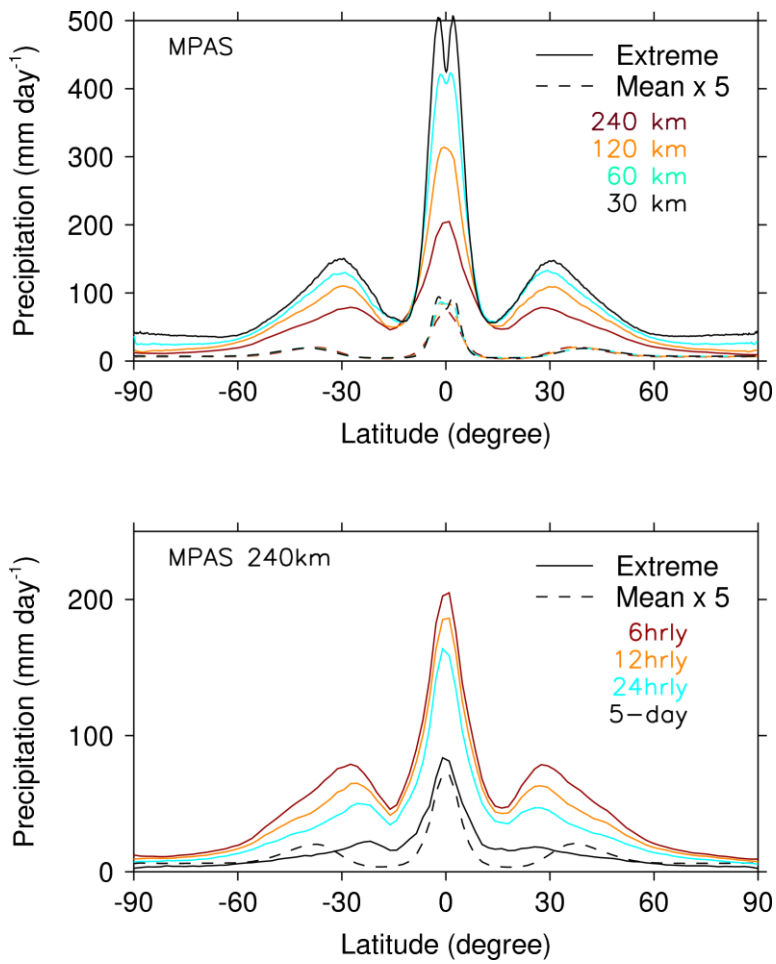

Figure 1: Latitudinal variations of mean and extreme (≥ 99.9th percentile of both wet and dry conditions) precipitation with the native grid resolution (panel a) and with different temporal data frequencies (6 hourly, 12 hourly, 24 hourly, and every 5 day) for the simulation at 240 km grid resolution (panel b). Due to the relatively small magnitudes, the mean values are scaled by a factor of 5 (Mean x 5; long dashed).

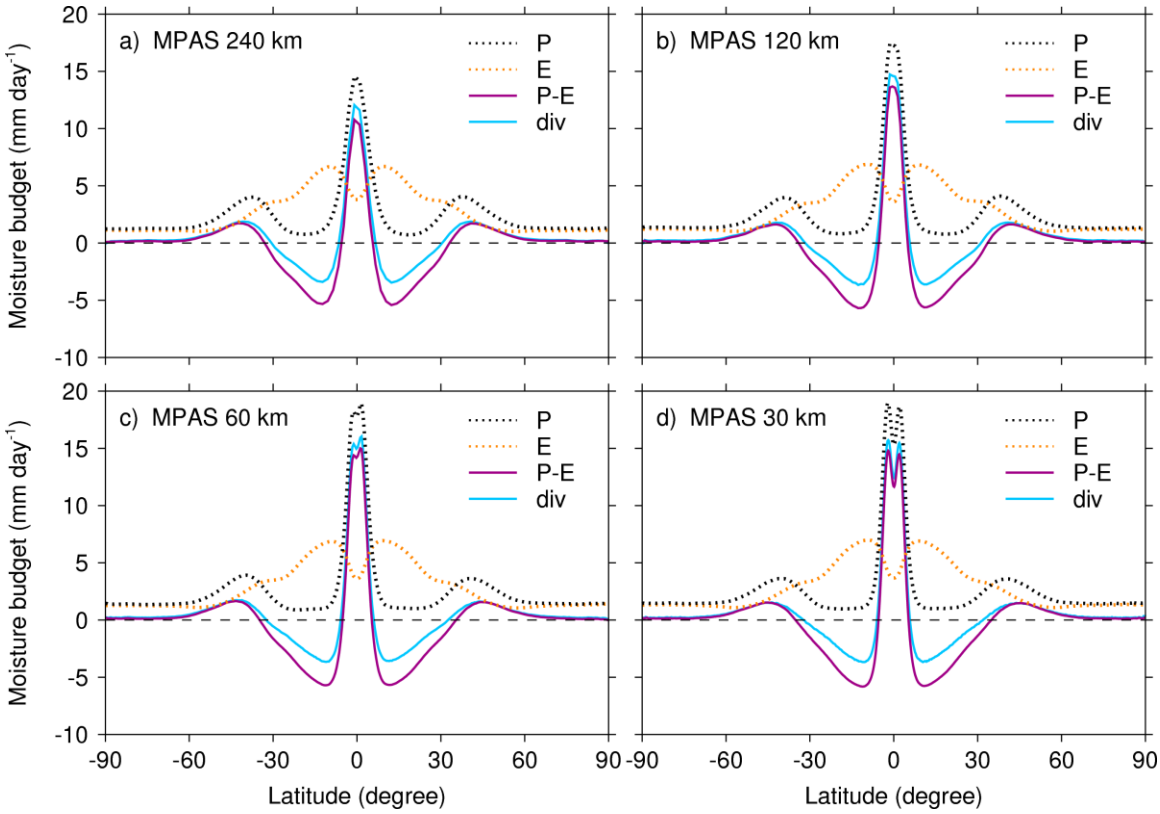

Figure 2: Meridional variations of mean moisture budget terms based on simulations using the MPAS-A dynamical core with 240, 120, 60, and 30 km native grid resolution (panels a, b, c, and d, respectively). The moisture budget terms include precipitation (P, black dashed), surface evaporation (E, yellow dashed), advective moisture convergence (div, blue solid), and P-E (purple, solid).

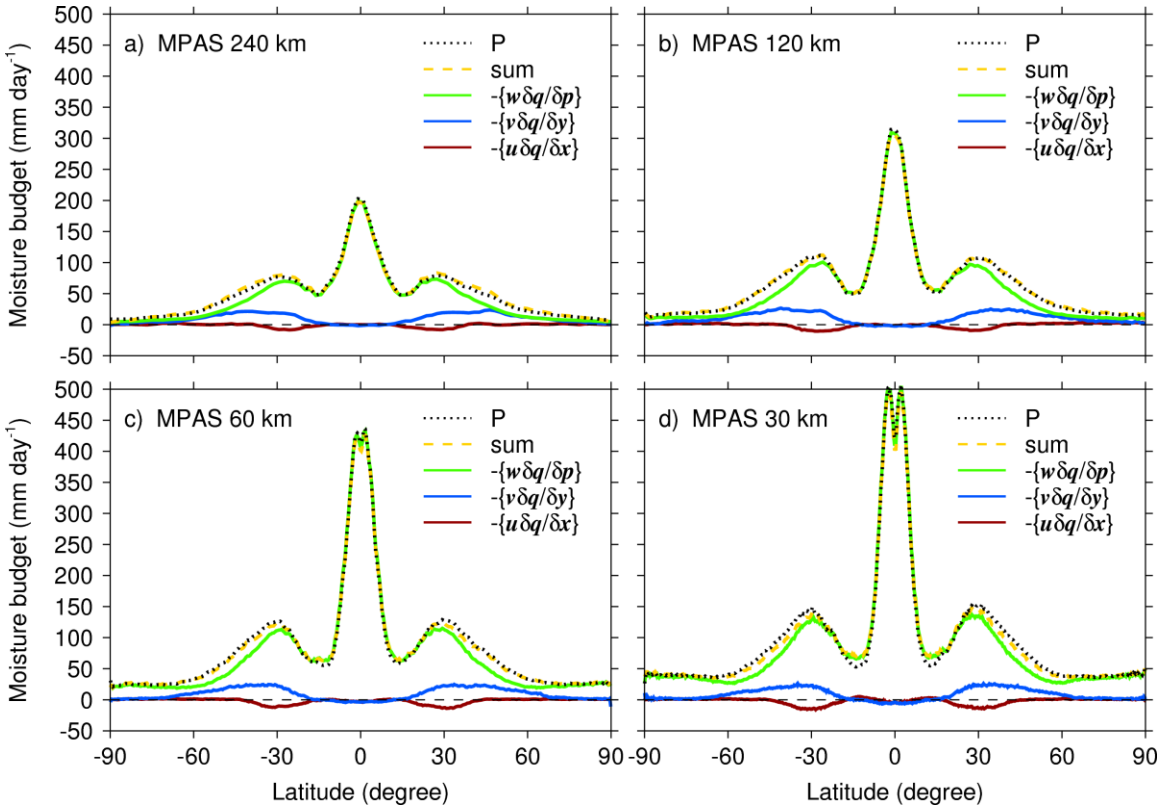

Figure 3: Meridional variations of moisture budget terms under extreme precipitation conditions based on simulations with the MPAS-A dynamical core and with 240 km, 120 km, 60km, and 30 km horizontal grid resolutions (panels a-d), respectively. Zonal, meridional and vertical advective moisture convergence during extremes, *{-uδq/δx}, {-vδq/δy}*, and *{-ωδq/δp},* are shown in solid brown, blue, and green lines along with the corresponding total advective moisture convergence (sum, yellow solid) and extreme precipitation (P, black dashed).

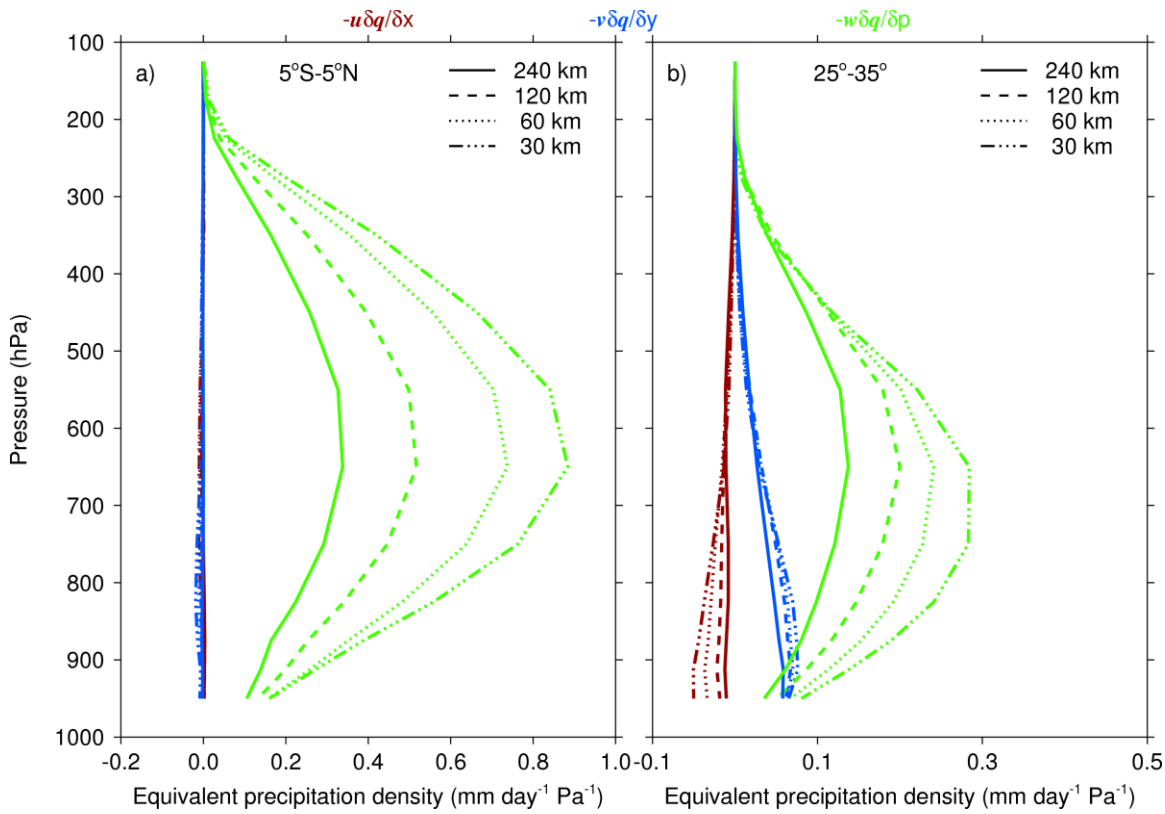

Figure 4: Vertical profiles of zonal (-*uδq/δx,* brown), meridional (-*vδq/δy,* blue), and vertical (-*ωδq/δp,* green) advective moisture convergence for simulations at their native grid resolutions of 30 (dash dot dot), 60 (dotted), 120 (dashed), and 240 km (solid) with the MPAS-A dynamical core for latitude bands of 5°S–5°N (left) and 25°–35° in both hemisphere (right).

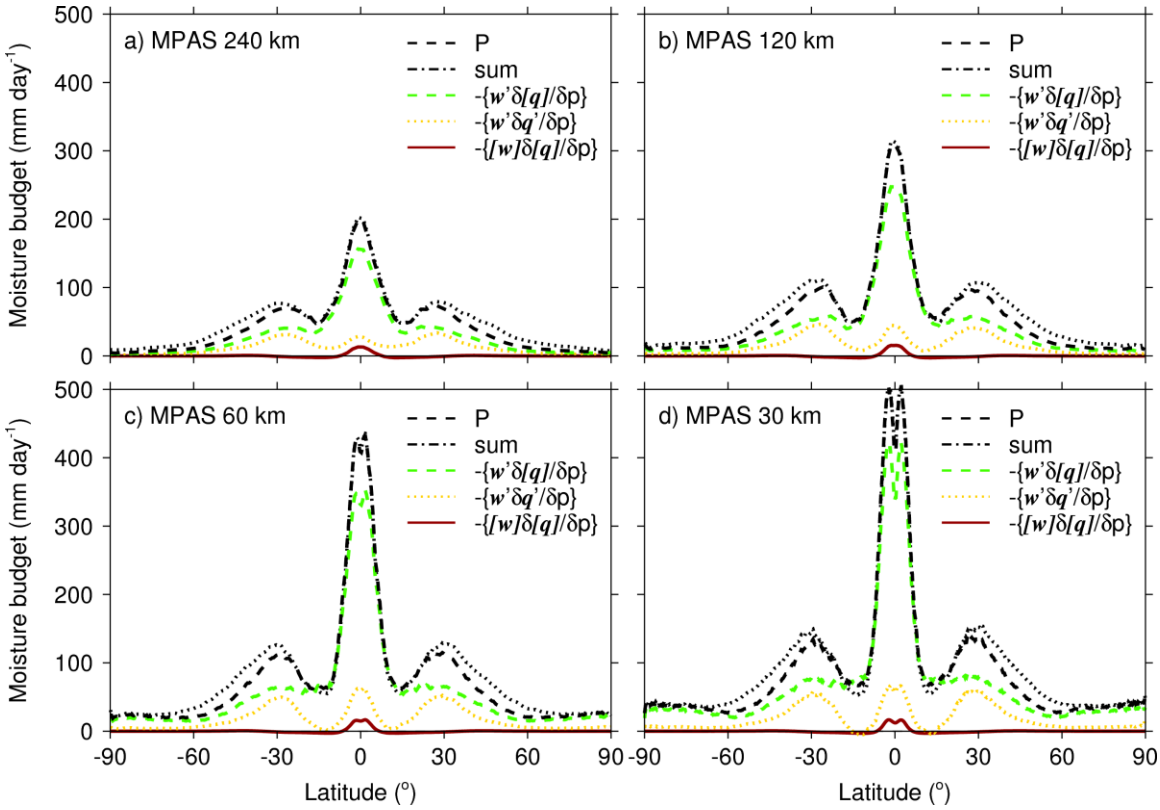

Figure 5: The breakdown of vertical advective moisture convergence during extremes into corresponding mean flow, {-*[ω]δ[q]/δp*} (brown solid), and two eddies related terms, *{-ω'δq'/δp}* (yellow dotted) and *{-ω'δ[q]/δp}* (green dashed), for the MPAS-A simulations at four native grid resolutions of 240, 120, 60, and 30 km. The total vertical advective moisture convergence (sum) and precipitation (P) during extremes are also shown as black dashed and dotted lines, respectively.

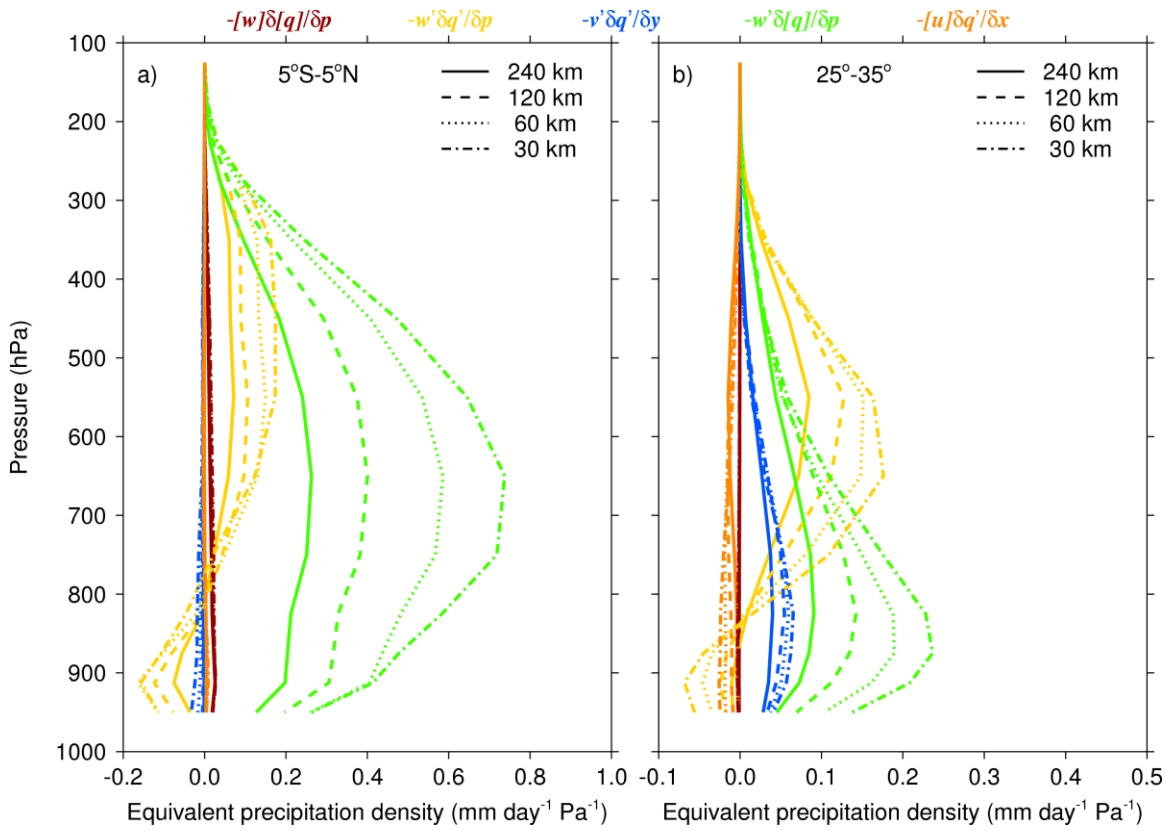

Figure 6: Vertical profiles of mean flow and eddy moisture transport for simulations at the native grid resolutions of 30 (dash dot), 60 (dotted), 120 (dashed), and 240 km (solid) with the MPAS-A dynamical core for the latitude bands of 5°S–5°N (Panel a) and 25°–35° (including both hemispheres, Panel b). The mean flow and eddies terms are too small and are omitted.

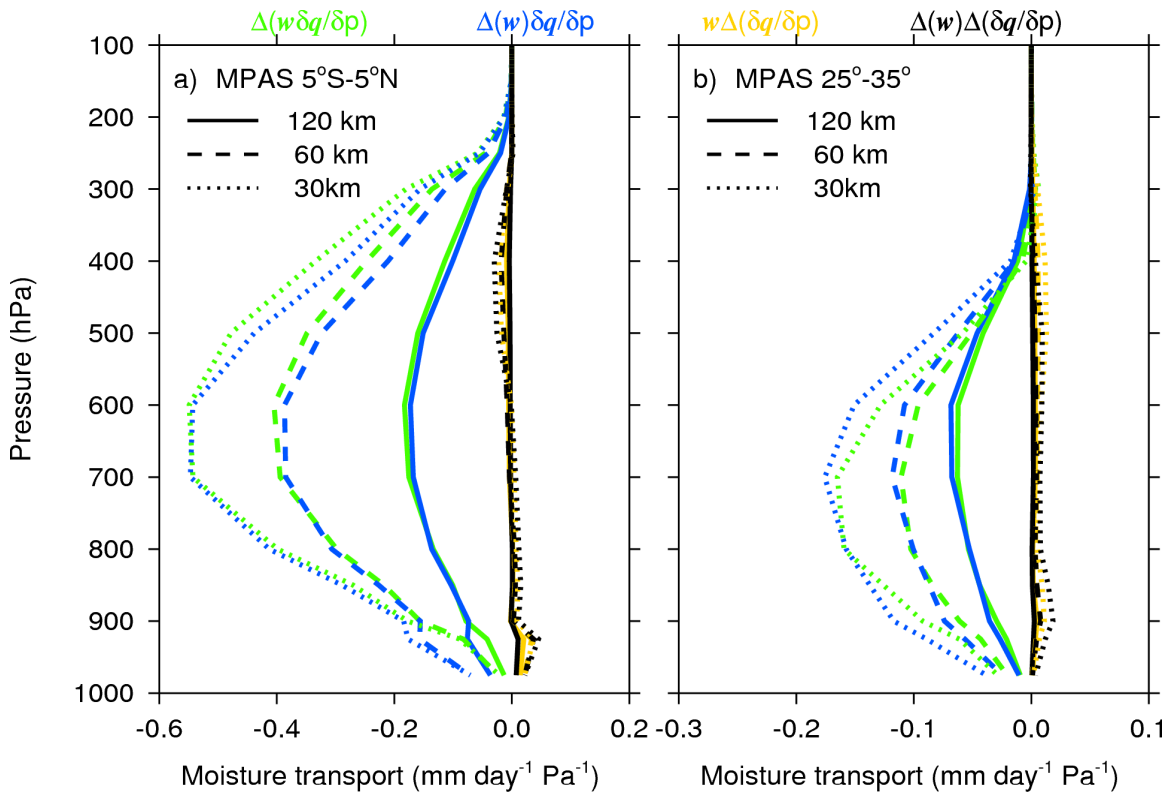

Figure 7: Estimated differences in vertical advective convergence ($\Delta(\omega\delta q/\delta p)$, green) between simulations at fine resolutions (30, 60, and 120 km) and that at the coarse resolution (240 km) during extremes, and the contributions to these differences by changes in dynamics ($\Delta(\omega)\ \delta q/\delta p$, blue), thermodynamics ($\omega\Delta(\delta q/\delta p)$, yellow), and their covariance changes ($\Delta(\omega)\Delta(\delta q/\delta p)$, black) relative to the coarse resolution (240 km). The estimates in this figure are based on simulations with the MPAS-A dynamical core and at their native grid resolution.

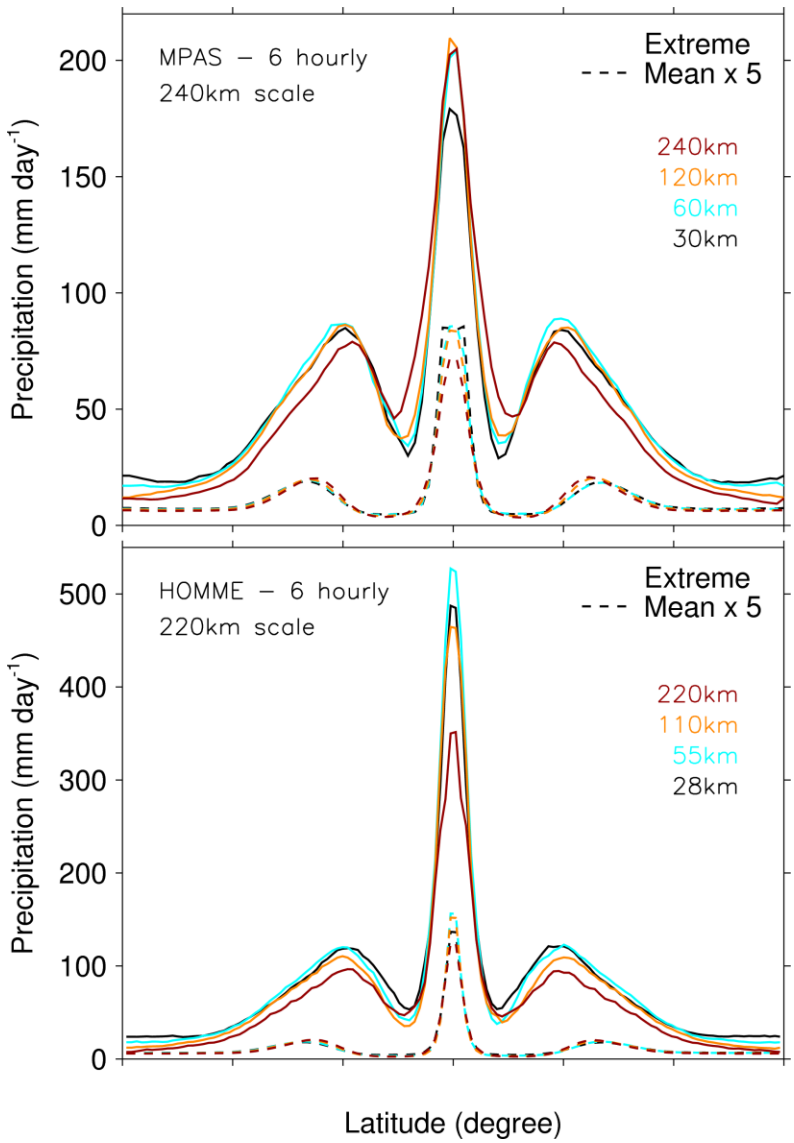

Figure 8: Variations of mean and extreme precipitation with grid resolution assessed at the same grid scale for simulations with the MPAS-A (Panel a) and HOMME dynamical cores (Panel b). The simulations conducted at fine resolutions have been aggregated (area-weighted averaged) to the coarse resolution grids (240 km for MPAS-A and 220 km for HOMME). The mean values are scaled by a factor of 5 (Mean x 5; long dashed) due to their relatively small magnitudes.

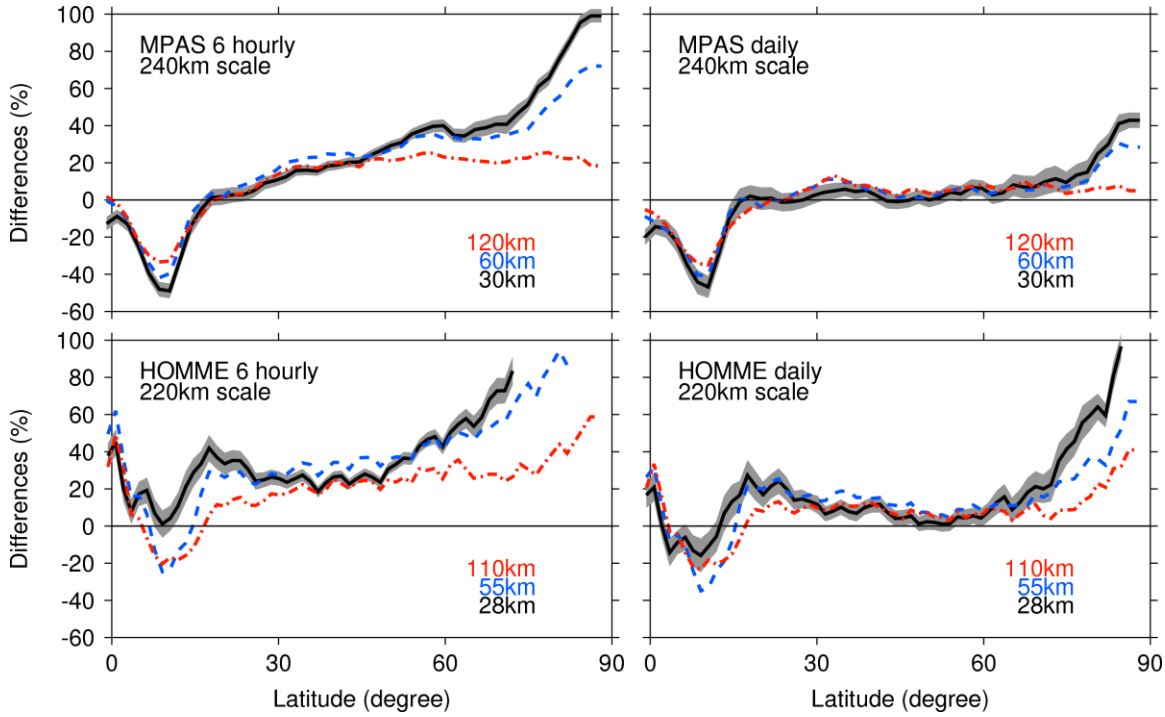

Figure 9: Differences of extreme precipitation between fine (120, 60 and 30 km for MPAS-A and 110, 55, and 28 km for HOMME) and coarse resolutions (240 km for MPAS-A and 220 km for HOMME) when assessed at the same grid using both 6 hourly (Panels a and c) and daily data (Panels b and d). The simulations conducted at fine resolutions have been aggregated (area-weighted averaged) to the coarse resolution grids (240 km for MPAS-A and 220 km for HOMME) before calculating the differences. The grey area indicates the 95% confidence interval within which the two fine resolution simulations are not statistically different.

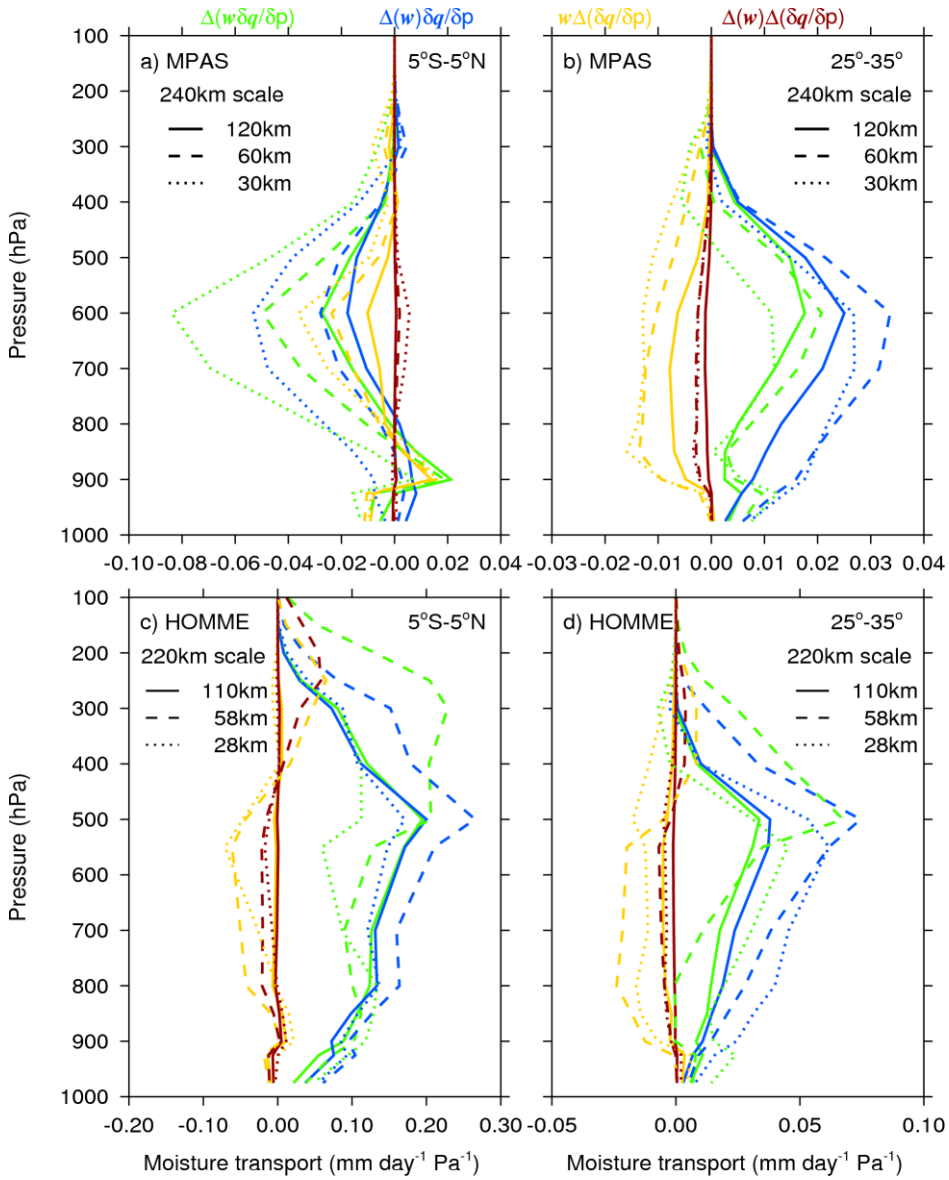

Figure 10: Contributions of dynamics ($\Delta(\omega)\delta q/\delta p$, blue), thermodynamics ($\omega\Delta(\delta q/\delta p)$, yellow), and their covariance changes ($\Delta(\omega)\Delta(\delta q/\delta p)$, black) to the scale dependency of vertical advective convergence ($\Delta(\omega\delta q/\delta p)$, green) for simulations with the MPAS-A (Panels a and b) and HOMME dynamical cores (Panels c and d). The changes are estimated as differences relative to the coarse resolution (240 km for MPAS-A and 220 km for HOMME) at the same grid scale.

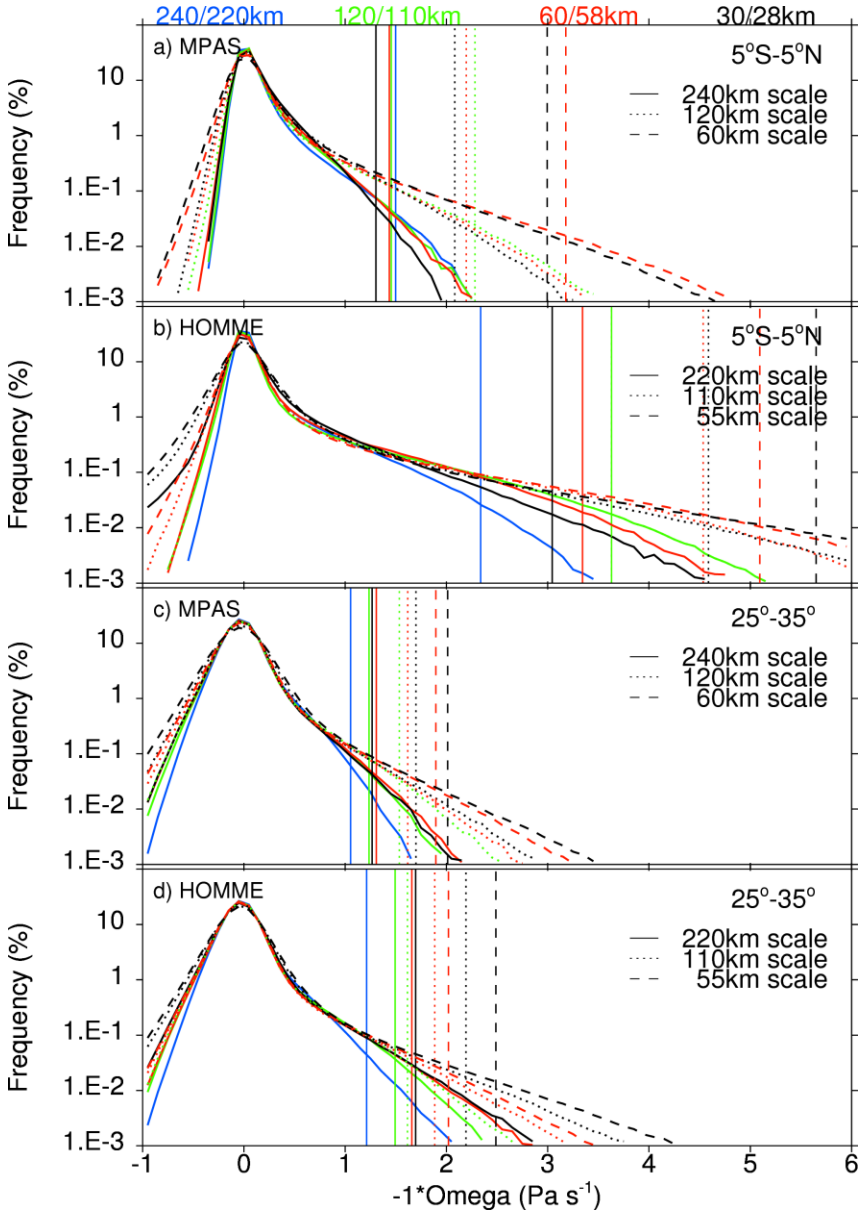

Figure 11: Resolution dependency of PDFs of -1*omega (on 600 hPa) for the 5°S–5°N (a, b) and 25°–35° (include both hemispheres) latitude bands (c, d). Colors indicate the native grid resolution the simulations were conducted. In the PDF, the different line styles indicate the coarse grid scale to which the fine resolution simulations have been aggregated, and the corresponding vertical line indicates the 99.9th percentile of the negative omega.

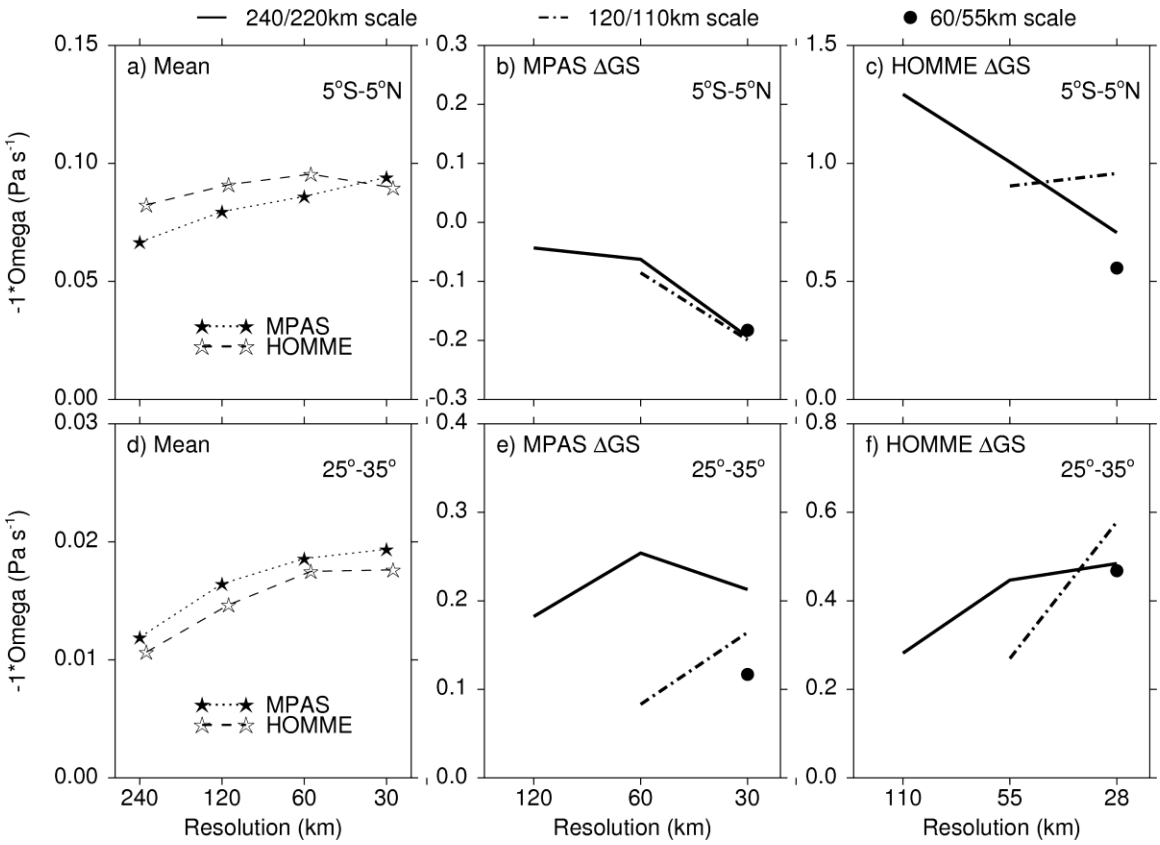

Figure 12: Mean negative omega (a and d) and the same grid differences (ΔGS) in 99.9th percentile of negative omega (b, c, e, and f) on 600 hPa for 5°S–5°N (top) and 25°–35° (include both hemispheres, bottom) latitude bands based on simulations with the MPAS-A or HOMME dynamical cores. The x-axis indicates the native grid resolution the simulations were conducted, and the solid line, dashed lines, and filled circle indicate the grid scales (240, 120, and 60 km for MPAS, respectively, and 220,110, and 55 km for HOMME, respectively) the fine resolution simulations were aggregated to for the grid scale comparison.